KSCE Journal of Civil Engineering 29 (2025) 100148

Contents lists available at ScienceDirect

KSCE Journal of Civil Engineering

journal homepage: www.elsevier.com/locate/kscej

Characteristics of ground motions in the Jeju Island during the 2021 M_L4.9 Jeju earthquake, South Korea

Youngkyu Cho [a], Seongnoh Ahn [a], Junyoung Lee [a], Jaehwi Kim [b], Byungmin Kim [a], Seokho Jeong [b,*]

[a] Department of Civil Urban Earth and Environmental Engineering, Ulsan National Institute of Science and Technology, Ulsan, 44919, South Korea
[b] Department of Civil Engineering, Changwon National University, Changwon, 51140, South Korea

ARTICLE INFO

Keywords:
Geology of volcanic island
Jeju earthquake
Magnitude and distance scaling of ground motion
Dynamic site characterization

ABSTRACT

An earthquake of local magnitude (M_L) 4.9 occurred on the southwestern seafloor of Jeju Island on December 14th, 2021. The geology of Jeju Island comprises granitic bedrock beneath a muddy marine sediment on top of which basalt and trachyte layers has formed, being expected to result in unique ground shaking characteristics. Analyzing accelerograms from eight seismic stations for 22 earthquakes, we explored intensity and frequency of ground motion and effects of earthquake source and path on ground motion intensity measures (IMs) across Jeju Island. Significantly higher ground motions were consistently recorded at several stations compared with other stations of similar source-to-site distances, indicating notable site amplification effects. Irrespective of seismometer installation depth, the dependence of IMs on M_L for $M_L \geq 3$ is typically analogous to the magnitude scaling of the existing ground motion models (GMMs). Dependence of IMs on source-to-site distance in Jeju Island indicates a relatively faster decay compared with mainland Korea, implying that the marine sediments between the granitic bedrock and basaltic island may strongly attenuate the surface ground motion amplitude. These findings highlight the necessity for a region-specific GMM and site effect models to effectively account for Jeju Island's distinctive ground motion characteristics in engineering applications.

1. Introduction

On December 14th, 2021, an earthquake of local magnitude (M_L) 4.9 earthquake occurred on the southwestern seafloor of Jeju Island, south of the Korean Peninsula. The cause of the earthquake was identified as seafloor fault activity. Despite its relatively small magnitude, this event caused considerable ground shaking (MMI scale = IV–V) on Jeju Island. Shaking on the island was the strongest ever recorded since the beginning of national instrumentation in 1978. Many people were alarmed and reported that the shaking was uncomfortable. However, because of the relatively infrequent occurrence of earthquakes in South Korea, insufficient data are available to understand the seismicity and ground motion characteristics in this region.

Following the mainshock, 21 aftershocks occurred over nine days near the epicenter. These aftershock data provide an opportunity to characterize low-intensity ground shaking and understand the influence of the earthquake source and path, offering valuable insights into this region for predicting the characteristics of potentially strong ground shaking triggered by moderate to large earthquakes in the future. Ahn et al. (2021) investigated the scaling effects of the magnitude and source-to-site distance on the ground motion intensity measure (IM) by utilizing ground motion records obtained from several seismic stations operated by the Korea Meteorological Administration (KMA) during the 2020 Haenam 74-earthquakes' swarm. Kwak et al. (2022) derived a local ground motion model (GMM) to predict within-rock motions by employing borehole records collected by Ahn et al. (2021). They compared the amplification factor (AF) estimated using the proposed GMM with AFs evaluated from site response analyses and other existing GMMs. Nizamani and Park (2021) evaluated the efficiencies of 14 existing GMMs developed for active shallow crustal, stable continental, and Korean regions in comparison with recorded data from the three largest earthquakes in Korea.

Until 2010, Jeju Island was considered safe from earthquakes. However, since then, >60 earthquakes with $M_L \geq 2$ have occurred near Jeju Island (as of Feb. 3rd, 2023), four of which had $M_L \geq 3$ after 2013. The recent development of tourism and consequent growth in the

---

* Corresponding author at: Department of Civil Engineering, Changwon National University, Changwon, Korea 51140.
E-mail address: seokho.jeong@changwon.ac.kr (S. Jeong).

https://doi.org/10.1016/j.kscej.2024.100148
Received 16 June 2024; Received in revised form 13 October 2024; Accepted 17 December 2024

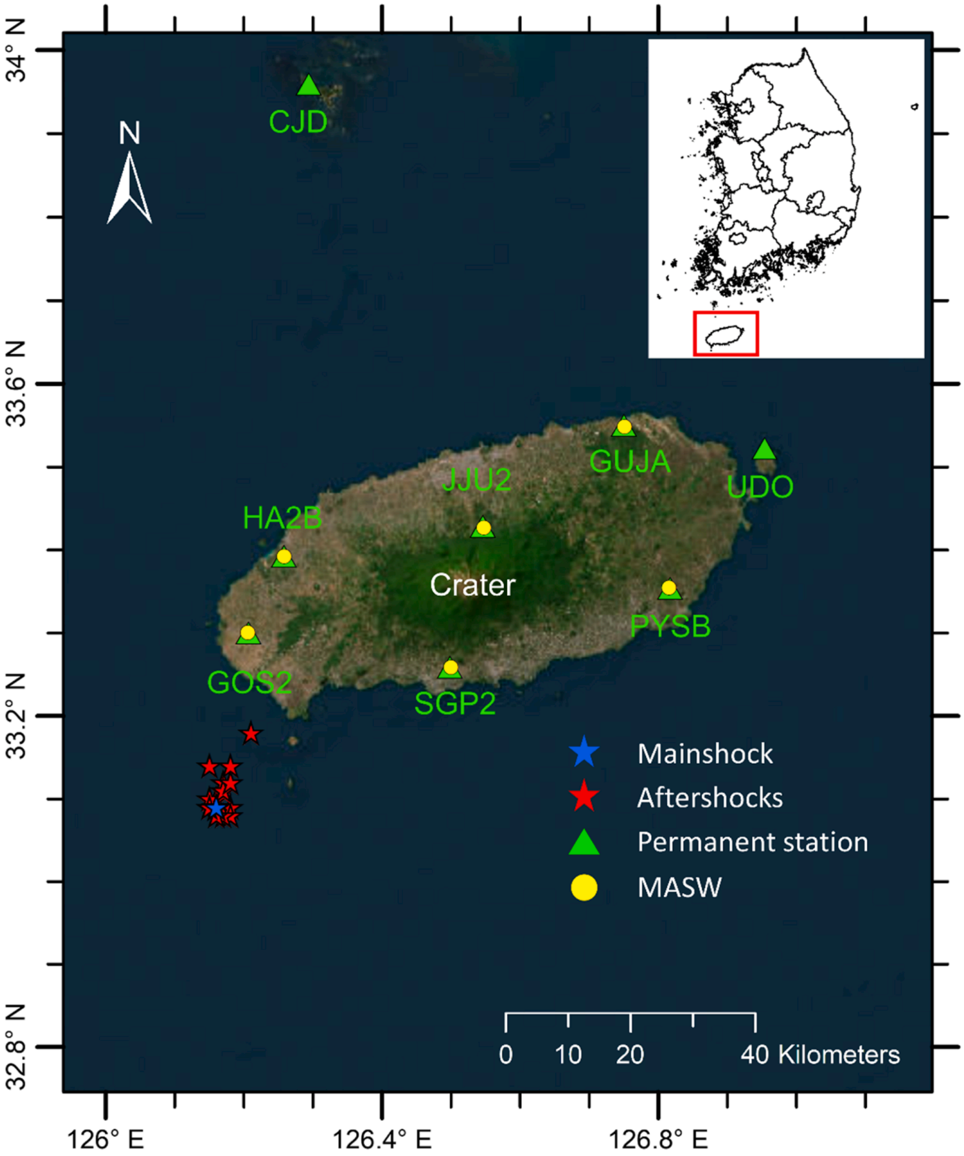

Fig. 1. Map displaying epicenters of 22 earthquakes, permanent seismic recording stations, and locations where MASW tests were performed.

residential population have led to a significant increase in infrastructure on the island. In light of these recent earthquakes and the increasing demand for infrastructure on Jeju Island, seismic design and site characterization for infrastructure construction must be performed based on the geology and geography of Jeju Island (Kim et al., 2021). However, Korean seismic design standards for infrastructure were proposed based on the geological and geotechnical characteristics of the Korean Peninsula, which significantly differs from those of Jeju Island; therefore, applying the standards to Jeju Island is questionable.

This study aims to investigate the characteristics of weak ground motions, specifically focusing on the scaling effect of magnitude and source-to-distance, utilizing the acceleration time series obtained from eight seismic stations of the KMA during the Jeju earthquake. The geology of Jeju Island was identified, and the shear wave velocity (V_S) profile and the horizontal-to-vertical spectral ratio (HVSR) were evaluated at eight stations. V_S refers to the velocity at which shear waves propagate, and the average shear wave velocity from surface to a depth of 30 m (V_{S30}) is often representative of the stiffness of the subsurface at a particular site. HVSR is related to the location of the bedrock, making it relevant to site characteristics as well. In total, 176 pairs of acceleration time series were collected, comprising the main shock and 21 aftershocks recorded at eight stations. We analyzed the acceleration time series for the mainshock and the response spectra for the entire earthquake in terms of the epicentral distance (R_{epi}) and V_{S30}. The predominant (T_p) and mean (T_m) periods averaged over the magnitude bins for each seismic station were evaluated. We estimated the rate of change for multiple intensity measures relative to the magnitude (i.e., the slope of the intensity measure with respect to the magnitude) and compared them with the coefficients derived from existing GMMs.

2. Study area

2.1. Jeju island

Fig. 1 shows Jeju Island, located south of the Korean Peninsula. An elliptical island, centered around a crater, was formed through volcanic activity. The volcanic activity period spanned approximately 1.8 Ma to the Holocene. Widespread and persistent hydrovolcanic activities deposited the Seogwipo Formation (around 1.8–0.5 Ma). From approximately 0.5 Ma to the Holocene, extensive volcanic activity on land built up the topographic framework and current configuration of Jeju Island with Halla Mountain (Woo et al., 2013; Koh et al., 2013).

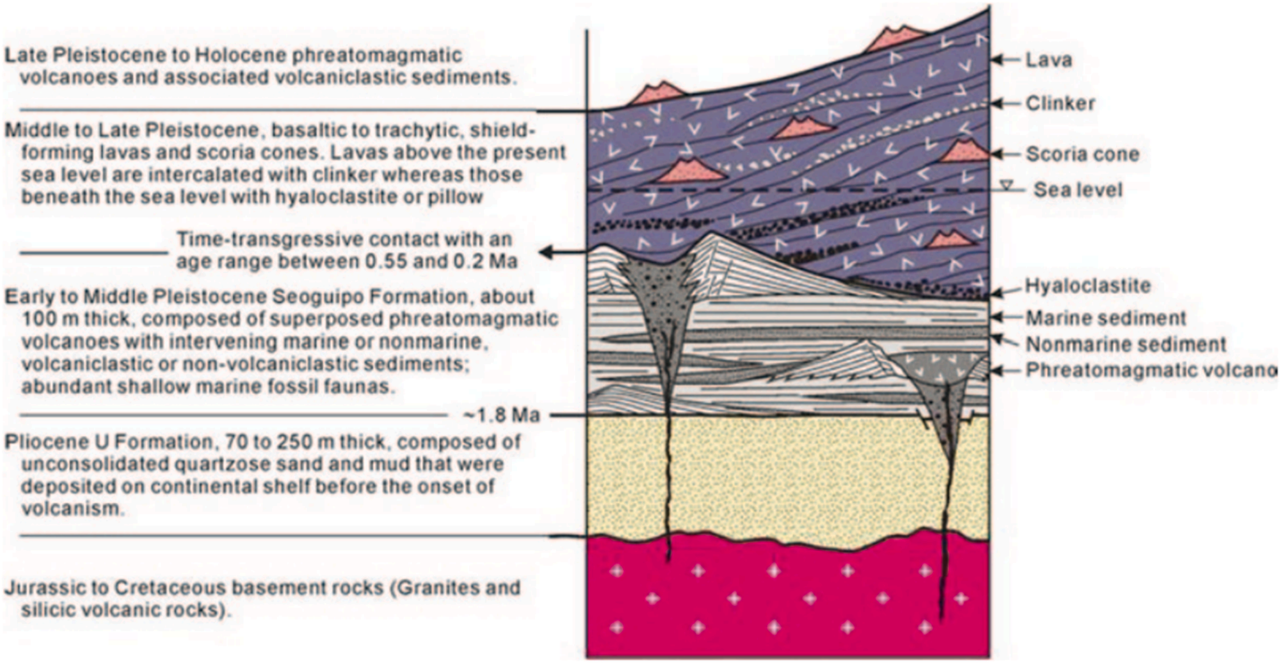

Fig. 2. Geology structure in Jeju Island (Woo et al., 2013).

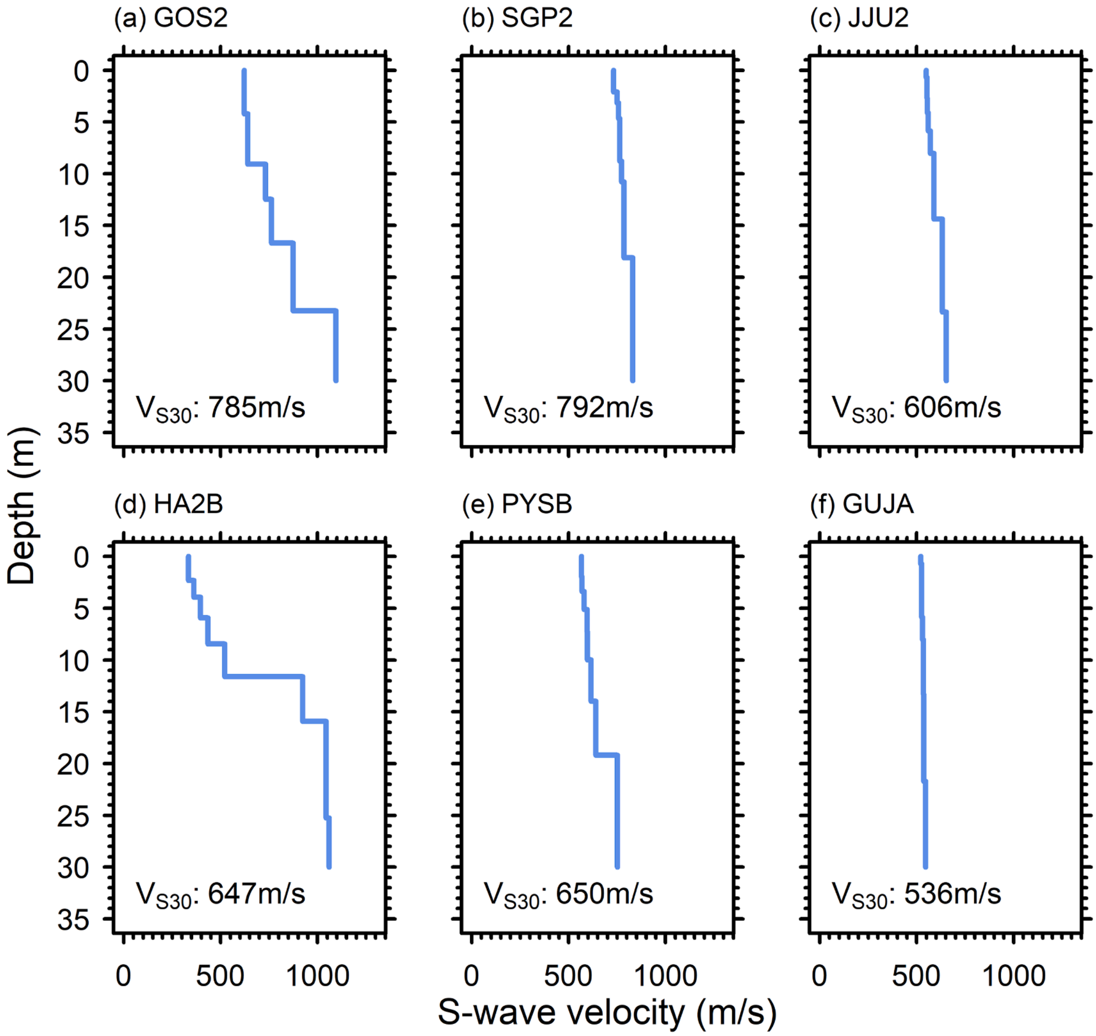

Fig. 3. V_S profiles at the six seismic stations.

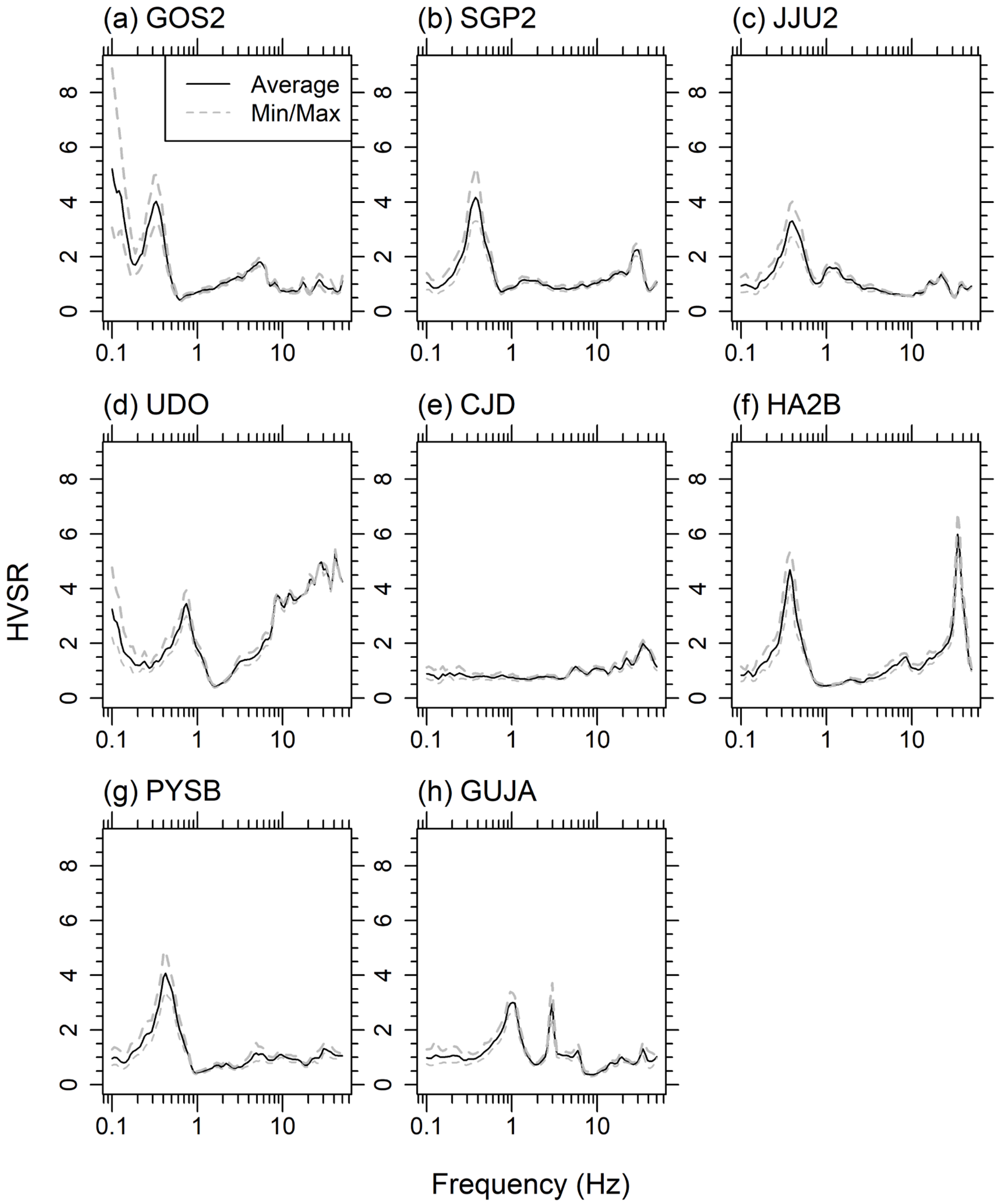

Fig. 4. HVSRs at the eight seismic stations.

Several islands created by parasitic volcanoes are located near the main island. The main island covers an area of approximately 1792 km^2, with a major axis of approximately 73 km in the east-northeast (ENE) direction and a minor axis of approximately 31 km in the north-northwest (NNW) direction. The slope of the main island along the major axis ranges from approximately 3 to 5°, whereas it is approximately 5° along the minor axis, which is slightly steeper than that along the major axis.

The geology of the island primarily consists of volcanic rocks that formed through the solidification of erupted magma, with volcanic ash distributed across the surface. The geological structure of Jeju Island, documented by Woo et al. (2013), is presented in Fig. 2. A summary of the detailed description of each geological layer is as follows: Granites and silicic volcanic rocks constitute the basement, which formed from the Jurassic to the Cretaceous. Above the basement, the Pliocene U Formation comprises unconsolidated quartzose sand and mud, with thicknesses ranging from 70 to 250 m. The U Formation is overlain by the Seogwipo Formation, which is approximately 100 m thick, and consists of volcaniclastic and non-volcaniclastic sediments. The Seogwipo Formation was formed during the Early to Middle Pleistocene. In addition to the Seogwipo Formation, there was a layer composed of basaltic to trachytic shield-forming lavas and scoria cones from the Middle to Late Pleistocene. In the superficial layer, volcaniclastic sediments formed during the Late Pleistocene and Holocene.

2.2. *Site characterization*

There are eight seismic stations operated by KMA on Jeju Island (Fig. 1). Five stations (CJD, GOS2, JJU2, SGP2, and UDO) had surface seismometers (ES-T-A). A surface seismometer was installed in a small temporary building with an exterior wall to minimize potential external

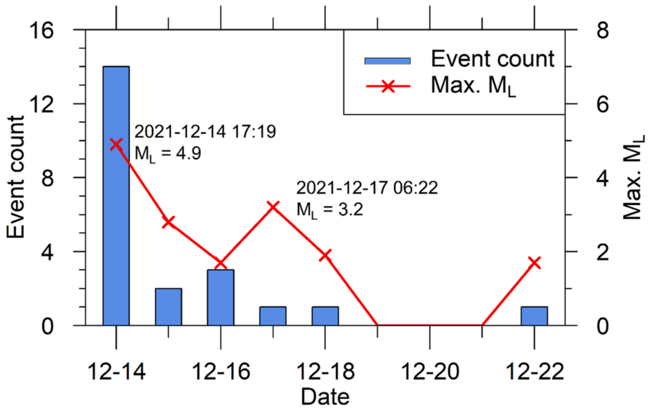

Fig. 5. Count of earthquake event and maximum magnitude in the period of the 2021 Jeju earthquake.

impacts. The remaining three stations (GUJA, HA2B, and PYSB) were equipped with seismometers (ES-DH-A) installed at a depth of approximately 100 m (borehole station). We obtained the V_S profiles at the sites of six KMA stations (GOS2, JJU2, SGP2, GUJA, HA2B, and PYSB) by performing a multichannel analysis of surface wave (MASW) test to estimate V_{S30}. During the test, we used 24 Geophones with a natural frequency of 4.5 Hz, linearly deployed at 2 m intervals. To obtain experimental dispersion curves, we measured the signals from active sources by striking a sledgehammer 10 times at a 10 m offset from both ends of a linear array (i.e., 10 stacks on each side). The experimental dispersion curves (i.e., phase velocities with a fundamental mode across a frequency) were extracted by picking the highest sum of amplitudes from the dispersion image produced by ParkSEIS (2016). The V_S profile was determined using the inversion algorithm proposed by Xia et al. (1999), which fits a theoretical fundamental mode dispersion curve derived from a layered ground model with assumed soil properties [including soil density, layer thickness, V_S, and primary velocity (V_P)] to the obtained experimental dispersion curve. Fig. 3 illustrates the V_S profiles along with the computed V_{S30} values at the six station sites. The V_S value is typically greater than 500 m/s at ground level, except for HA2B station, and gradually increases to greater than 800 m/s at stations other than JJU2, PYSB, and GUJA. Additionally, a V_S value of approximately 760 m/s is mostly observed at a depth of approximately 15 m, except at GUJA station. As we could not conduct MASW test at CJD and UDO stations, we predicted the V_{S30} values at each station's site using the P-wave seismogram methods proposed by Kim et al. (2016). The method estimates the average shear-wave velocity to a certain depth of z (V_{SZ}) using the ratio of the radial to the vertical component of the initial portion of P-wave seismograms and converts it to V_{S30} using the V_{SZ}-V_{S30} relationship. The application of this method to Korea was validated by Kim et al. (2020) and Lee et al. (2022).

Using three-component ambient-noise measurements available from the eight stations, we estimated the HVSR using the Geopsy software. The HVSR exhibits a clear, first peak value when soil-to-rock boundary has a prominent average impedance contrast in the sedimentary deposit. The frequency corresponding to the clear, first peak HVSR is analogous to the fundamental frequency of a site (Nakamura, 1989). The HVSR can be readily analyzed from the horizontal and vertical components of an ambient-noise record at a single seismometer. We can infer an approximate trend of V_S profile and a depth-to-competent rock at a site from the HVSR measurement (Vantassel et al., 2018; Kim et al., 2023). SESAME (2004) provides the comprehensive instructions on the measurement and application of the HVSR. We applied the smoothing method of Konno and Ohmachi (1998) to ambient noise signals sampled in the Fourier amplitude spectrum at frequencies ranging from 0.1 to 50 Hz. Fig. 4 illustrates the minimum, mean, and maximum HVSRs across the frequencies evaluated at the eight station sites. Except for CJD, which is located >50 km from Jeju Island, the obtained HVSR displays a well-defined peak at a frequency of < 1 Hz. In contrast, the HVSR at CJD is flat at a frequency of < 10 Hz. The frequencies corresponding to the first spike of HVSR are lower than 0.5 Hz for GOS2 (0.32 Hz), SGP2 (0.38 Hz), JJU2 (0.40 Hz), HA2B (0.38 Hz), and PYSB (0.41 Hz), except for UDO (0.71 Hz), and GUJA (1.0 Hz). Considering the geological history of Jeju Island, the presence of unconsolidated quartzose sand and mud beneath the volcanic rock is presumed to have resulted in these long-period oscillations (> 2 s). The seismometers at HA2B, PYSB, and GUJA are located inside boreholes, but all these stations show low-frequency ambient vibrations comparable to those of other surface stations.

3. 2021 December 14th M_L4.9 Jeju earthquake

Fig. 5 depicts the number of earthquake occurrences recorded between December 14th and 22nd, 2021 along with their corresponding maximum magnitudes. A total of 22 earthquakes with magnitudes ranging from 1.3 to 4.9 were recorded during this period. The main shock occurred in the ocean southwest of Jeju Island on December 14th, 2021 (Fig. 1). 13 aftershocks were recorded on the day of the mainshock, which was the highest number of occurrences during this period. Subsequently, eight other aftershocks occurred within approximately one week. The epicenters of the 21 aftershocks were within a radius of 10.5 km centered around the epicenter of the mainshock, and their focal depths ranged from approximately 8.0 km to 19.0 km. Notably, two of these aftershocks had M_L greater than 2.0.

4. Ground motion characteristics

All seismometers recorded ground shaking in three directions [East-West (EW), North-West (NS), and Vertical)] and had a sampling rate of 100 Hz. We collected 176 pairs of acceleration time series for the three directions recorded at eight stations during the 22 earthquakes from the National Earthquake Comprehensive Information System (NECIS) (Korea Meteorological Administration, 2013) to understand the ground shaking characteristics. The ground-motion records were preprocessed through a baseline correction and a band-pass Butterworth filter. The band-pass Butterworth filter requires high- and low-pass cutoff frequencies. We applied a low-pass cutoff frequency of 30 Hz to all the records. The high-pass cutoff frequency of each record was determined as the frequency at which the Fourier amplitude of the seismogram intersects three times the Fourier amplitude of the ambient noise. The noise part of each record was distinguished based on the P-wave arrival time detected using an algorithm proposed by Kalkan (2016). When the Fourier amplitude of the seismogram was significantly greater than three times the Fourier amplitude of the noise without intersections, a high-pass cutoff frequency of 0.1 Hz was used. Records with a derived high-pass cutoff frequency higher than 5 Hz were excluded.

Fig. 6 shows the acceleration time series of the three directions recorded at the eight stations for the mainshock along the seismometer types, R_{epi}, V_{S30}, and PGA. The V_{S30} values for the eight stations range from 600 to 800 m/s. Of note, we observed that the PGAs at JJU2 station are greater than those at SGP2 station for the surface seismometer, although JJU2 (R_{epi} = 52 km) station was farther away from the mainshock epicenter than SGP2 (R_{epi} = 37 km) station. For instance, the ratios of PGA at JJU2 to PGA at SGP2 stations are 2.33 (EW), 1.49 (NS), and 1.12 (Vertical). A similar trend in the ratio is also observed for the other earthquakes [namely, 1.07 (EW), 1.30 (NS), and 1.61 (Vertical) for the No 6 event in Table 1; and 1.84 (EW), 1.79 (NS), and 1.06 (Vertical) for the No 16 event in Table 1]. Interestingly, PGAs for the three directions at CJD station are greater than those at UDO station [i.e., the ratios of PGA at CJD to PGA at UDO stations: 2.86 (EW), 2.26 (NS), and 2.52 (Vertical) for the mainshock; 2.50 (EW), 3.00 (NS), and 2.33 (Vertical) for No 15 event in Table 1; and 3.33 (EW), 2.80 (NS), and 1.77 (Vertical) for No 16 event in Table 1]. It is believed that the different

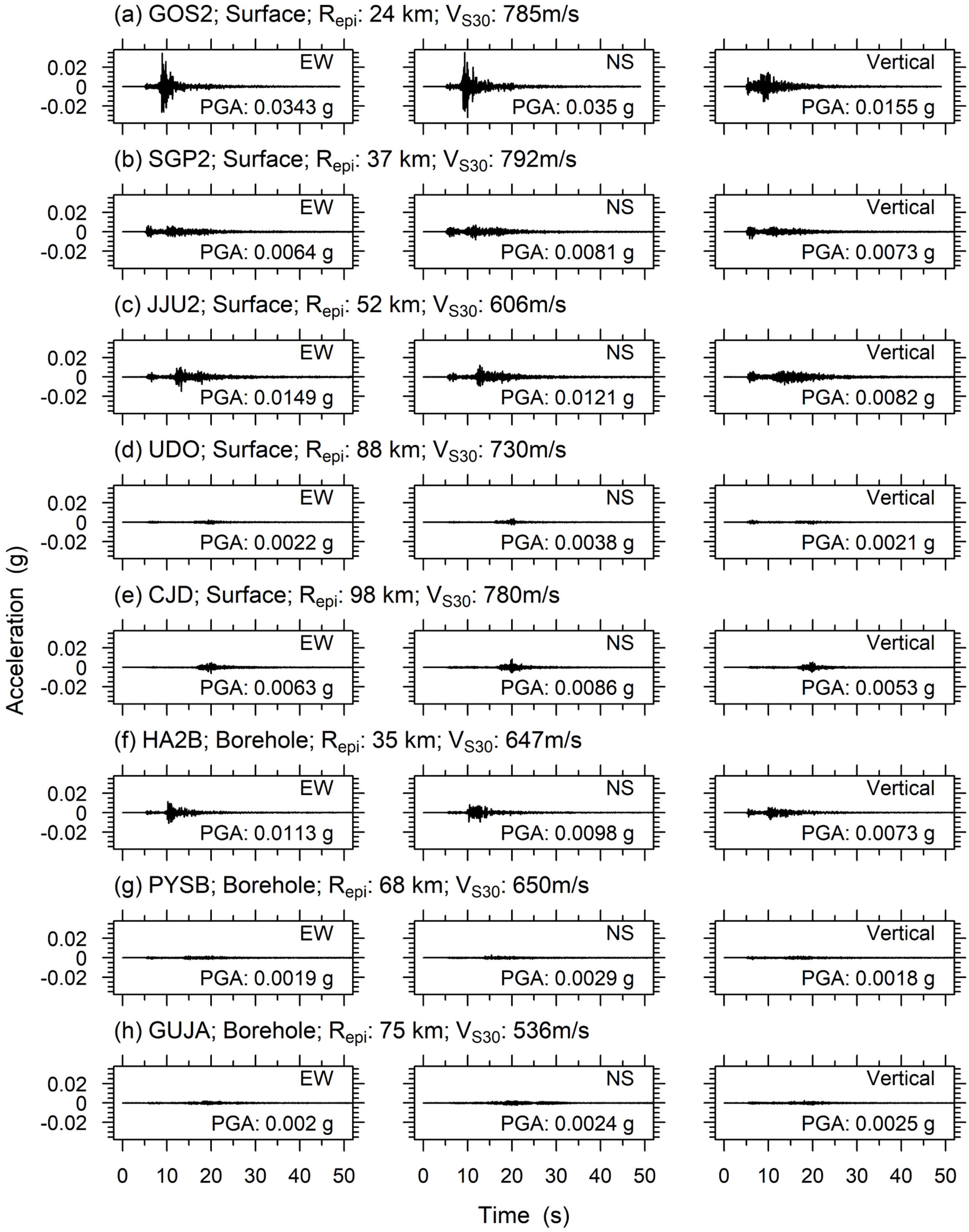

Fig. 6. Acceleration-time series in EW, NS, and Vertical directions during the main shock recorded at: (a) GOS2 station, (b) HA2B station, (c) SGP2 station, (d) JJU2 station, (e) PYSB station, (f) GUJA station, (g) UDO station, and (h) CJD station.

geological characteristics of the two islands may result in distinct PGAs, which will be discussed in "Section 7".

Fig. 7 illustrates the 5 % damped acceleration response spectra of the processed ground motion records at the eight stations. N in each panel represents the number of processed ground motion records available at each station. The spectral acceleration from the mainshock at GOS2 station (surface type), closest to its epicenter among the surface type stations, is the greatest at periods of approximately 0.20 s, 0.25 s, and 0.15 s for the EW, NS, and Vertical directions, respectively. At HA2B station (closest to the epicenter among the borehole stations), the peak values of spectral acceleration from the same earthquake appear at a period of around 0.08 s, 0.22 s, and 0.18 s for the EW, NS, and Vertical directions, respectively. With M_L diminishing, a decrease in spectral acceleration across all seismic stations is observed.

We computed T_p, which represents a spectral period corresponding to the greatest spectral acceleration, and T_m, the inverse of the frequency averaged by a weighting factor of a squared Fourier amplitude by Rathje et al. (1998), for the 74 pairs of processed, horizontal ground motion

Table 1
Date of earthquake occurrence, earthquake magnitude, and coordinates of earthquake epicenter.

No.	Date	M_L	Latitude (° N)	Longitude (° E)	Focal depth (km)
1	2021–12–14 17:19	4.9	33.09	126.16	17
2	2021–12–14 17:29	1.3	33.08	126.16	15
3	2021–12–14 17:29	1.5	33.12	126.17	8
4	2021–12–14 17:36	1.7	33.10	126.16	18
5	2021–12–14 18:02	1.6	33.10	126.16	18
6	2021–12–14 18:23	1.7	33.09	126.15	17
7	2021–12–14 18:24	1.6	33.09	126.18	12
8	2021–12–14 19:02	1.5	33.10	126.15	10
9	2021–12–14 19:08	1.6	33.09	126.18	16
10	2021–12–14 19:14	1.6	33.10	126.15	17
11	2021–12–14 20:45	1.3	33.08	126.18	16
12	2021–12–14 22:02	1.5	33.09	126.15	17
13	2021–12–14 22:03	1.5	33.08	126.17	15
14	2021–12–14 22:36	1.3	33.08	126.16	14
15	2021–12–15 09:32	1.7	33.09	126.15	17
16	2021–12–15 15:06	2.8	33.14	126.15	14
17	2021–12–16 00:16	1.7	33.11	126.17	17
18	2021–12–16 05:01	1.4	33.18	126.21	9
19	2021–12–16 21:03	1.4	33.11	126.17	13
20	2021–12–17 06:22	3.2	33.12	126.18	18
21	2021–12–18 23:50	1.9	33.09	126.16	16
22	2021–12–22 21:14	1.7	33.14	126.18	19

records. T_p and T_m are the parameters that describe the frequency contents of ground motion. Rathje et al. (1998) showed that T_m characterizes the low-frequency content of ground motion better than T_p. Each period was averaged across the M_L bins for each station, as shown in Fig. 8. Both T_p and T_m mostly increase with increasing M_L, consistent with the fact that the low-frequency contents of ground motions generally become prominent as the earthquake magnitude increases. $T_m \geq 0.1$ s is observed from all stations for the earthquake with $M_L > 3$, whereas T_p is greater than or close to 0.1 s for $M_L > 3$, except for PYSB and SGP2 stations.

5. Source effect

The influence of the earthquake source on the ground shaking levels was investigated by examining the relationship between the M_L and IMs derived from the processed horizontal acceleration time series for the eight stations, as depicted in Figs. 9 and S1–S3 in the Electronic Supplementary Material. Four intensity measures were considered: PGA; peak ground velocity (PGV); acceleration response spectrum (Sa) at the oscillating period of 0.2 s ($Sa^{0.2s}$); and Sa at the oscillating period of 1 s (Sa^{1s}). Although the number of data points diminishes with M_L, the logarithmic PGAs in Fig. 9 are weakly and strongly correlated with M_L for $M_L < 3$ and $M_L \geq 3$, respectively, except for UDO station. The PGAs linearly increase with M_L up to a particular M_L value, a hinge point, beyond which the increasing rate decreases except for UDO and GUJA stations (i.e., The slope for $M_L < 3$ is mostly steeper than that for $M_L \geq 3$ in the six stations). A similar trend is observed in the plots of PGV and $Sa^{0.2s}$ against M_L, as shown in Figs. S1 and S2. Of note, the slopes for Sa^{1s} in Fig. S3 exhibit a contrasting pattern compared with those observed in PGA, PGV, and $Sa^{0.2s}$ (i.e., the slope for $M_L < 3$ is generally smaller than that for $M_L \geq 3$ at GOS2, SGP2, JJU2, CJD, HA2B, and GUJA stations).

Using bi-linear fitting, we computed the slopes of the four IMs in natural logarithms against M_L (magnitude scaling) at $M_L < 3$ and $M_L \geq 3$ for each station. Figs. 10 and 11 show statistics (i.e., median, 25 and 75 percentiles, minimum, maximum, mean, and mean ± one standard deviation) of the slopes for the four IMs for the surface and borehole stations, respectively. The median values of the slopes for PGA, PGV, $Sa^{0.2s}$, and Sa^{1s} at $M_L < 3$ are 2.55, 2.77, 2.86, and 2.17, respectively, for surface stations (Fig. 10a). For the borehole stations, these values are 2.49, 2.8, 2.94, and 1.96 at $M_L < 3$, respectively (Fig. 11a). At $M_L \geq 3$, the median values of the slope for PGA, PGV, $Sa^{0.2s}$, and Sa^{1s} are 1.4, 1.89, 1.84, and 2.49, respectively, for the surface stations (Fig. 10b), with similar values computed for the borehole stations (Fig. 11b). This trend of different magnitude scaling values in the two M_L ranges reflects observation made by Ahn et al. (2021). These calculated slopes for $M_L \geq 3$ were compared with the magnitude scaling term of existing GMMs. Six GMMs were considered: four NGA-West2 GMMs (Abrahamson et al., 2014; Boore et al., 2014; Campbell & Bozorgnia, 2014; Chiou & Youngs, 2014) and two GMMs proposed by Emolo et al. (2015) and Yun et al. (2008) based on database in South Korea. Hereafter they are abbreviated as ASK14, BSSA14, CB14, CY14, Emolo15, and Yun08. In the existing NGA-West2 GMMs, M_W is used as the magnitude term, but in this study, M_L was used to determine the magnitude scaling with the NGA-West2 GMMs. Sheen et al. (2018) introduced an improved equation for calculating M_L for the KMA and showed that M_W and M_L values are comparable. As described in Table 2, for BSSA14, CB14, CY14, and Emolo15, the source terms are separable from path and site terms; thus, it is possible to calculate source scaling directly. However, for ASK14 and Yun08, the source terms are not distinguishable from the path terms. Therefore, in this study, we obtained the IM by the source term using six GMMs considering the source-to-site distance and calculated the slope of the IMs against M_L.

The magnitude scaling relationships of NGA-West2 GMMs were reasonably consistent with the observed ground shaking during the aftershock sequence for $M_L \geq 3$, although they were based on overseas data. Specifically, for the surface stations (Fig. 10b), the ranges (a distance between maximum and minimum values in the boxplot or mean ± one standard deviation) of computed slopes of PGA, PGV, and $Sa^{0.2s}$ vs. M fall within the dispersion in the magnitude scaling of the six GMMs. For Sa^{1s}, the interquartile range and mean ± one standard deviation of computed slopes of Sa^{1s} are covered by the variability in the dispersion in the magnitude scaling of the six GMMs. For the borehole stations (Fig. 11b), the spreads of computed slopes of PGA, PGV, $Sa^{0.2s}$, and Sa^{1s} vs. M are comparatively smaller than the scatters in the magnitude scaling of the six GMMs due to fewer number of stations relative to the surface stations.

6. Path effect

The source-to-site distance has been incorporated into all GMMs as a primary predictor to account for geometric spreading and anelastic attenuation, which decrease ground shaking levels as a function of source-to-site distance. This phenomenon is often referred to as a path effect. To evaluate the path effect, we analyzed the relationship between

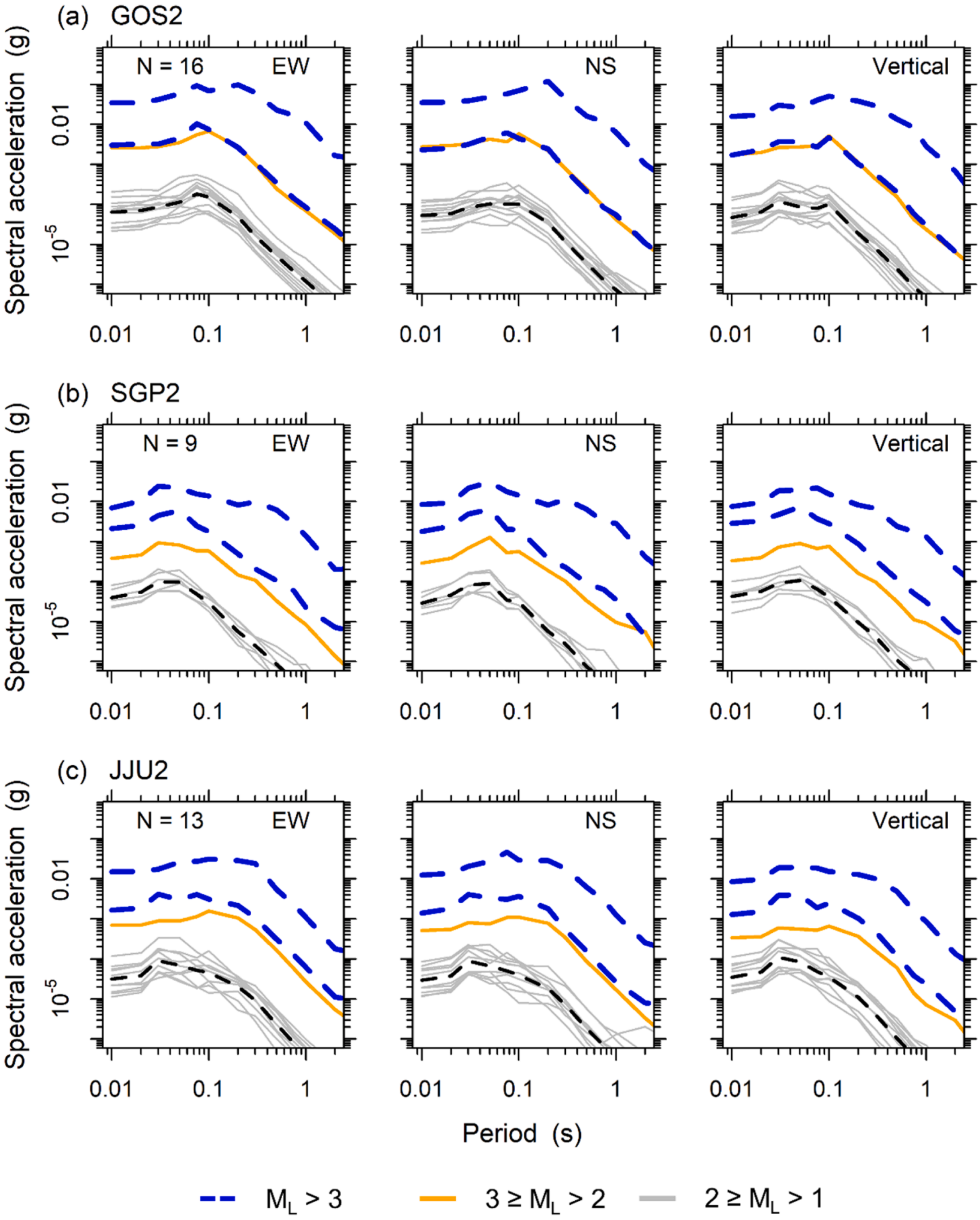

Fig. 7. 5 % damped acceleration response spectra of available postprocessed acceleration records from the 26 original acceleration records in EW, NS, and Vertical directions for the period of the 2021 Jeju earthquake: (a) GOS2 station, (b) HA2B station, (c) SGP2 station, (d) JJU2 station, (e) PYSB station, (f) GUJA station, (g) UDO station, and (h) CJD station. (Black dashed line refers to average of the spectra for $M_L \leq 2$).

the hypocenter distance (R_{hypo}) and the four IMs of records from the eight seismic stations during the 2021 Jeju earthquake in semi-log space, with only IMs on a logarithmic scale. Linear fitting (distance scaling) for the surface and borehole stations was conducted, respectively. Fig. 12 displays the computed slopes of the four IMs versus R_{hypo} plotted against M_L for the surface stations. The slopes for PGA range from −0.050 to −0.014 with small dispersions, as indicated by the statistical lines. Solid and dashed lines represent the mean (= −0.025) and mean ± one standard deviation (= 0.0091), respectively. The slopes for PGV, $Sa^{0.2s}$, Sa^{1s} exhibit similar distributions to those for PGA (excluding one significant outlier for Sa^{1s}). Fig. 13 illustrates the computed slopes of the four IMs versus R_{hypo} plotted against M_L for the borehole stations. The slopes for PGA range from −0.020 to −0.085 with moderate dispersions, as denoted by the mean (= −0.046) and mean ± one standard deviation (= 0.024). Similar distributions are observed in the slopes for PGV, $Sa^{0.2s}$, and Sa^{1s} as compared with those for PGA.

We present box plots for the slopes of the four IMs for distance scaling for both surface and borehole stations, respectively, (see Fig. 14) and compared these slopes with the coefficients of the six existing GMMs (i.e., the distance scaling term). Yun08 and Emodo15 adopted the epicentral distance (R_{epi}) as the source-to-site distance variable, while ASK14, BSSA14, CB14, and CY14 employed the closest distance to

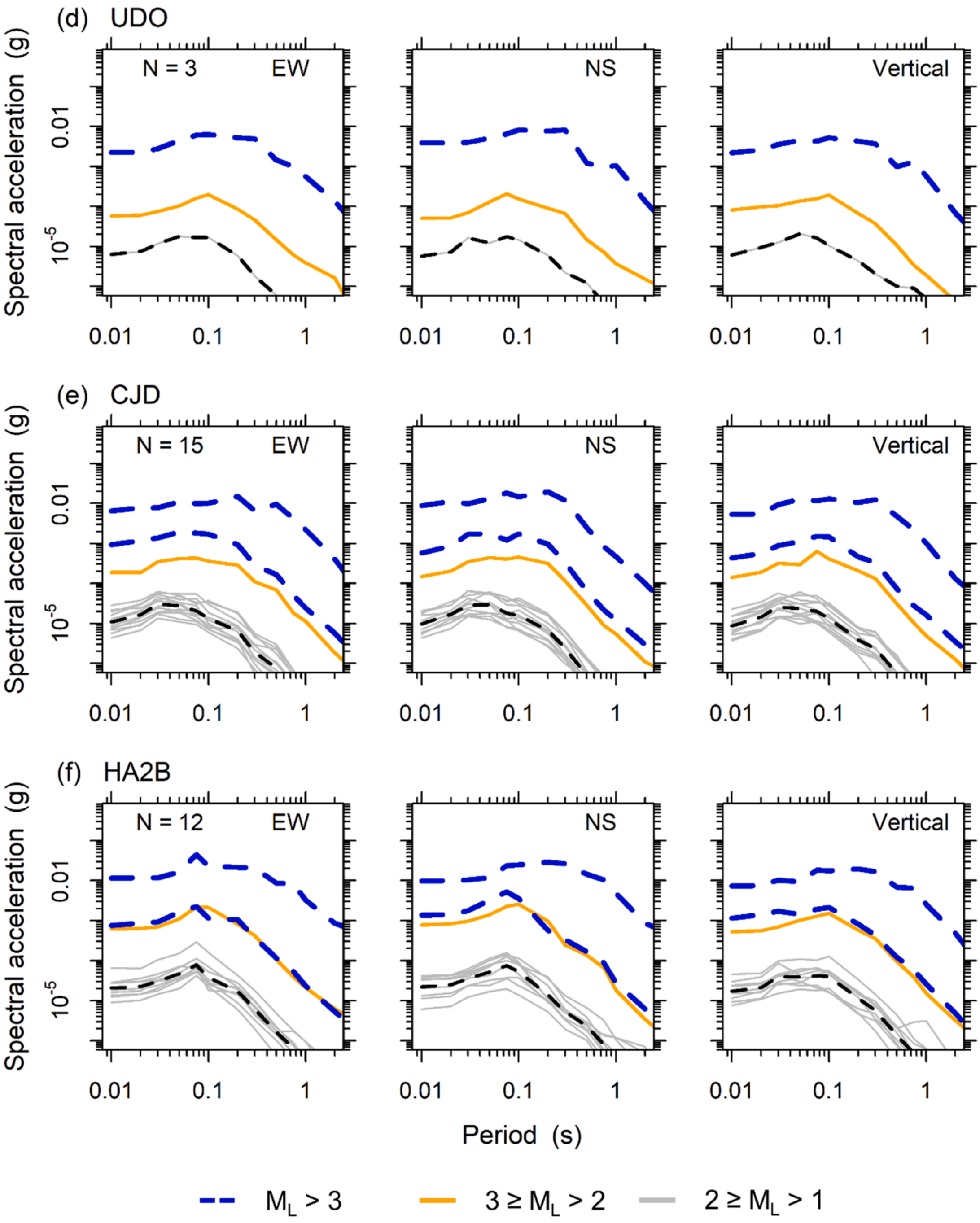

Fig. 7. (*continued*).

coseismic rupture (R_{rup}) or the closest distance to the surface projection of coseismic rupture (known as Joyne-Boore distance, R_{JB}) as the source-to-site distance variable to explain the path effect. The main shock occurred via the strike-slip fault, and the areas of the rupture plane were small for earthquakes with small magnitudes. Consequently, we computed the median value of the four IMs, assuming that R_{hypo} and R_{epi} are the same as R_{rup} and R_{JB}, respectively. The six GMMs did not exhibit a simple linear relationship for distance scaling. Hence, we fitted the predicted slopes with the linear lines in the six GMMs with respect to R_{hypo} to compare the slopes of the data calculated as the ratio of IM and R_{hypo}. The distributions of computed slopes of for IMs vs. R_{hypo} for the surface stations (Fig. 14a) are comparable to those of the coefficients from six GMMs except that the range for Sa1 s are far wider than that of the six GMMs. For the borehole stations (Fig. 14b), the mean or median values of calculated slopes of PGA, PGV, and $Sa^{0.2s}$ vs. R_{hypo} are mostly smaller than those of the six GMMs' coefficients. Whereas Sa^{1s} shows a similarity in the mean or median between the calculated slopes and the coefficients of the six GMMs.

7. Discussion and conclusions

The 2021 M_L4.9 Jeju earthquake was one of the most remarkable events that occurred on the Korean Peninsula since the beginning of national seismic instrumentation, followed by dozens of aftershocks that occurred in a clustered pattern. This event offers an opportunity not only to validate GMMs derived from databases in Korea but also to improve these models. The geology of Jeju Island consists of granitic bedrock covered by layers of loose sediments (Seogwipo and U formations), with

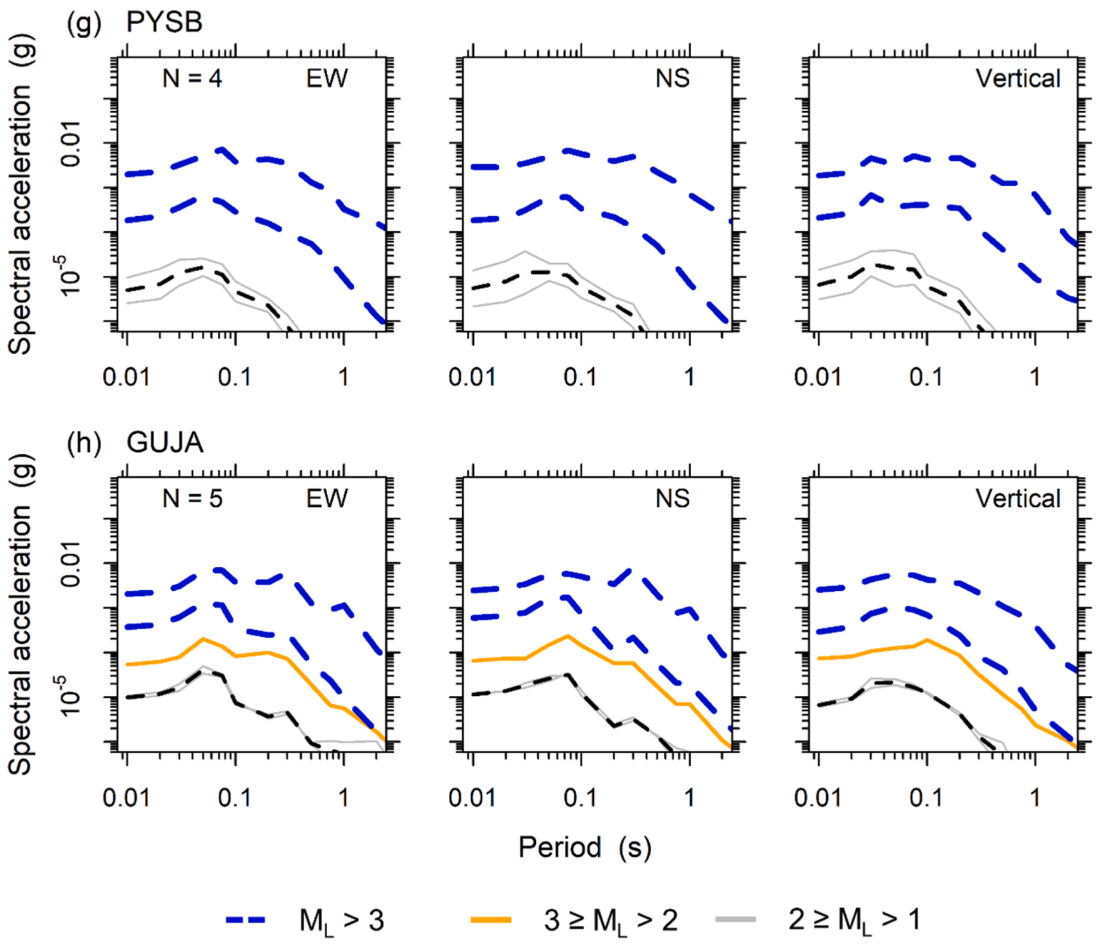

Fig. 7. (*continued*).

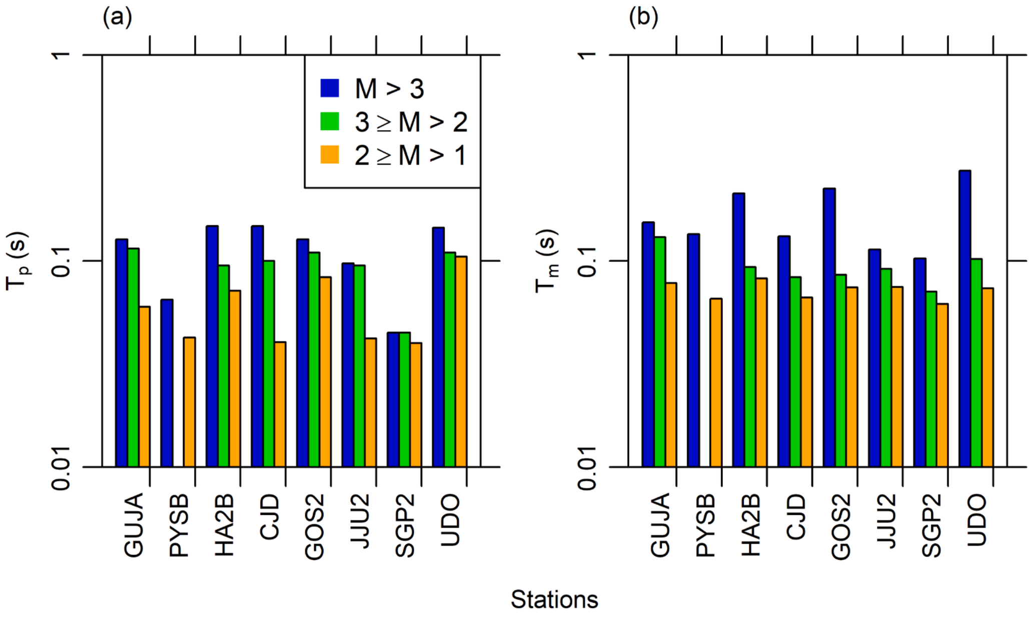

Fig. 8. The averaged values of (a) Tp and (b) Tm of horizontal ground motions recorded at the eight stations.

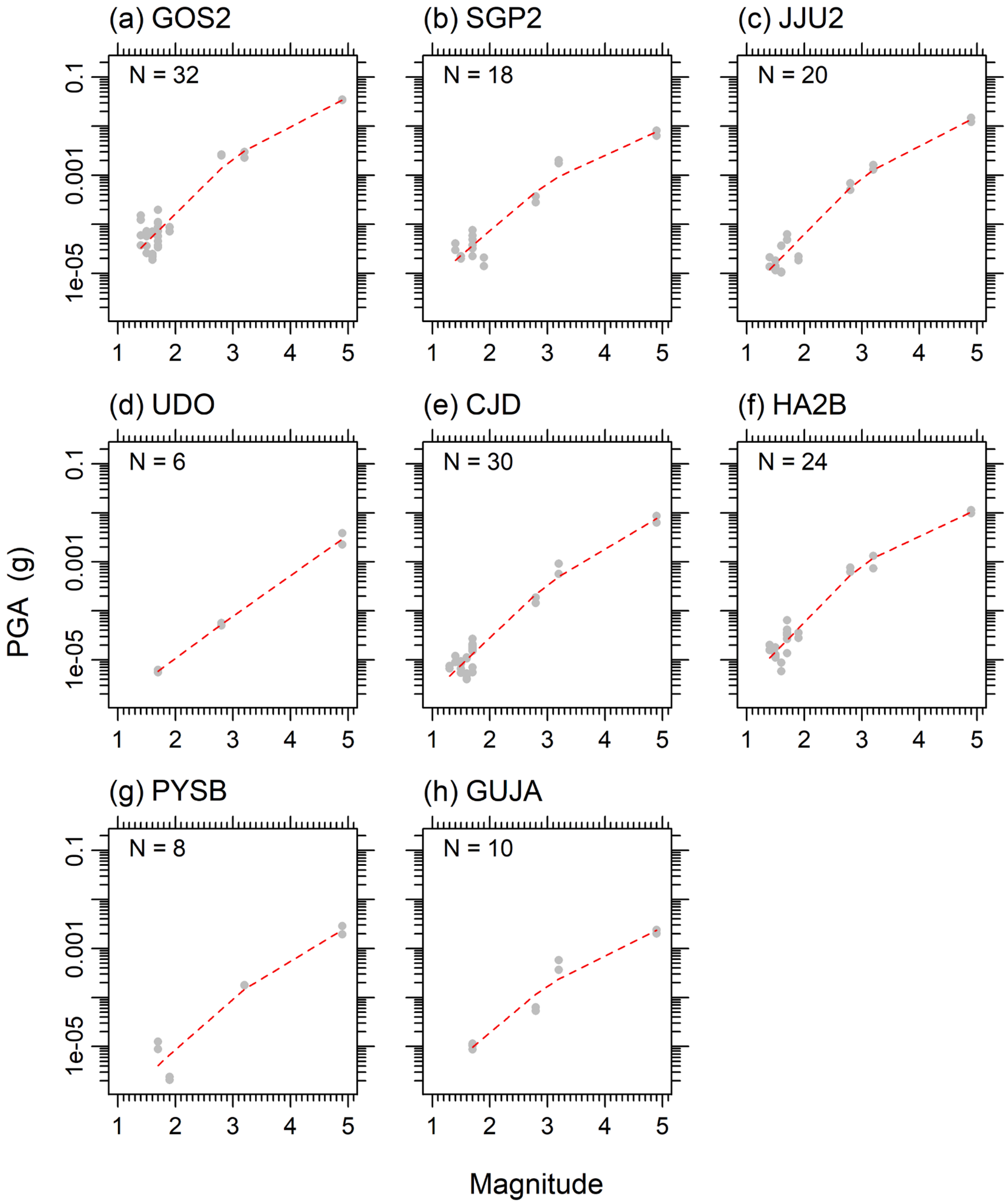

Fig. 9. Relationship between PGA and M_L at the eight stations.

basalt and trachyte layers forming on top as a result of volcanic activity. This unique geological composition appears to influence seismic wave propagation. We analyzed the characteristics of ground shaking, including intensity and frequency content, using the accelerograms recorded at the permanent stations for 26 earthquakes. We also studied the V_S structures and HVSR at the station sites to investigate the influence of local geology on the observed ground motions, and further explored the relationship between the ground shaking levels and the earthquake source and path.

Recorded ground motions showed a relatively large variability that can't be easily explained by the source and path effects. Shallow Vs profiles and HVSR do not explain this variability either. Fig. 6 shows the acceleration time series recorded during the mainshock, which clearly showed this variability. For example, the PGAs recorded at JJU2 station were much larger than those recorded at SGP2 station. The EW component was more than twice larger, even though JJU2 was 15 km farther away from the mainshock epicenter than the SGP2 station. The PGAs recorded at HA2B were larger than at SGP2 even though HA2B was inside a borehole and SGP2 was on the ground surface. Source-to-site distances were very close for those two stations. There could be many factors contributing to this observed variability of ground shaking, such as the complexity in the wave propagation or the local amplification of ground motion due to the small-scale variability in the structure of the volcanic island. Developing a high-resolution 3D velocity model of the island may help reduce this variability in the future, but without such a model one will need to account for the observed variability in the ground motion prediction.

Despite being closer to the epicenter, the ground motions recorded at UDO station showed consistently smaller PGAs than those recorded at CJD station. The geology at CJD station is known to be similar to that of the Korean Peninsula (Kim et al., 2006). However, the geologic characteristics at UDO station is expected to be similar to Jeju Island,

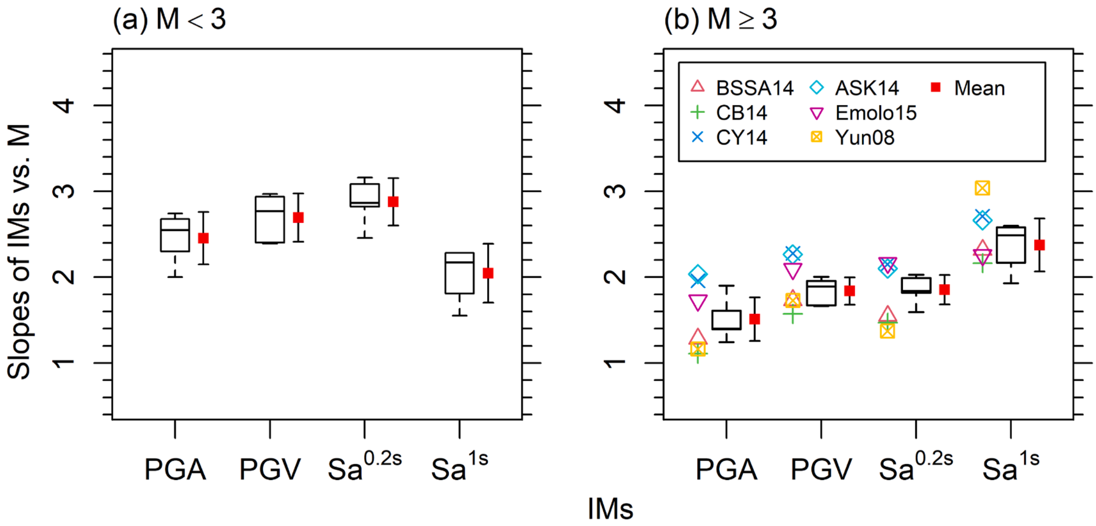

Fig. 10. Statistics for the slopes of magnitude against the four intensity measures (i.e., PGA, PGV, $Sa^{0.2s}$, Sa^{1s}) for (a) $M_L < 3$ and (b) $M_L \geq 3$. (Surface stations: GOS2, SGP2, JJU2, UDO, and CJD).

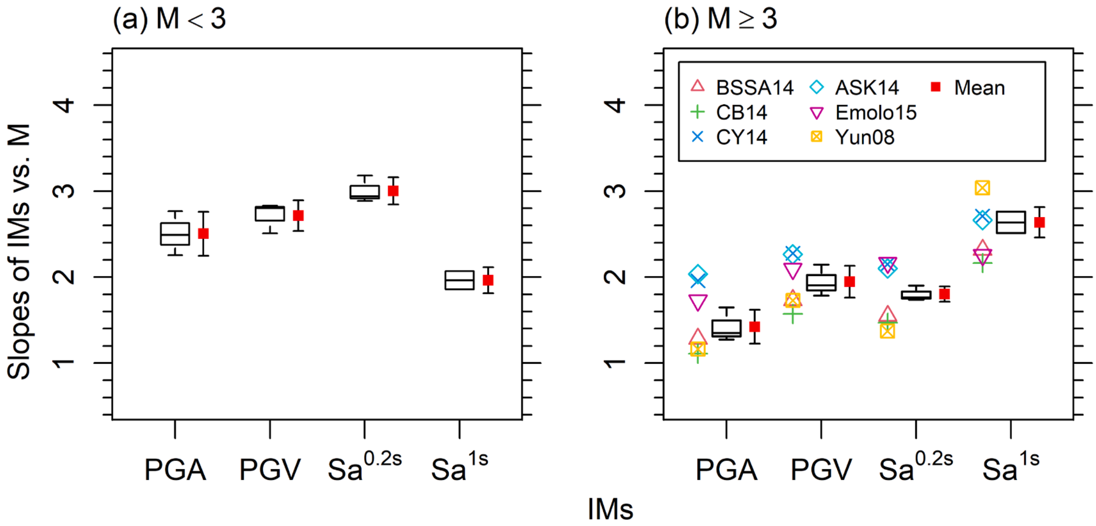

Fig. 11. Statistics for the slopes of magnitude against the four intensity measures (i.e., PGA, PGV, $Sa^{0.2s}$, Sa^{1s}) for (a) $M_L < 3$ and (b) $M_L \geq 3$. (Borehole stations: HA2B, PYSB, and GUJA).

containing the Seogwipo and U Formations. It is inferred that these two formations may have influenced the reduction in the amplitude of seismic waves propagating toward the ground surface within the Jeju Island. The influence of Seogwipo and U Formations is demonstrated by the HVSR and V_{S30} measurements. Jeju Island is primarily composed of basalt and trachyte to a depth of about 50 - 100 m below the ground surface, with an unconsolidated soft soil layer (Seogwipo and U formations) located beneath it. Considering that the V_{S30} value exceeds 500 m/s, Jeju Island generally comprises rocks in the subsurface; however, the HVSR peaks for GOS2, JJU2, SGP2, and UDO were observed to be well below 1 Hz, which is influenced by the Seogwipo and U formations. Whereas CJD near the inland Korea presents HVSR peak at approximately 6 Hz, which suggests shallow sediments overlying bedrock. Our study suggests that the free vibration of the Jeju Island is dominated by the compliance of Seogwipo and U formation sandwiched between the basement and the volcanic island and that the ground motions at Jeju Island may be consistently smaller than in mainland Korea.

It was observed that the slopes of IMs against M_L estimated from our measurements for $M_L \geq 3$ were comparable to the distributions in the regression coefficients associated with the magnitude scaling of the existing GMMs, regardless of the seismometer installation depth. This implies that the magnitude scaling for this sequence of events is unbiased from common tendencies for the earthquakes with $M_L \geq 3$. Whereas the slopes for $M_L < 3$ were steeper than those for $M_L \geq 3$. The change in magnitude scaling across different magnitude ranges, as described above, is also reflected in the functional forms of several existing GMMs (ASK14, BSSA14, and CB14), which exhibit changes in the moderate-to-large magnitude range (4.0–7.25). In the case of the Korean local GMMs (Yun08 and Emolo15), the change in magnitude scaling according to the magnitude is not reflected. However, a bilinear pattern was observed in the range of small magnitudes, with a hinge at $M_L = 1.8$ for the ground motions recorded during the 2020 Haenam earthquake swarm in South Korea (Ahn et al., 2021).

The slopes of IMs vs. R_{hypo} at the surface stations were overall similar

Table 2

Functional form of the source term for the three considered GMM.

GMM	Source term	Magnitude range
CB14	$f_{mag} = c_0 + c_1 M_W$ where c_0 and c_1 are period dependent regression coefficients.	$M_w \leq 4.5$
CY14	$c_0(M_W - 6) + \frac{c_2 - c_3}{c_n} \ln(1 + \exp(c_n(c_M - M_W)))$ where c_2, c_3, c_n, c_M are period dependent regression coefficients.	–
Emolo15	$a + bM_L$ where a and b are period-dependent regression coefficients.	–
ASK14	$f_1 = a_1 + a_4(M_2 - M_1) + a_8(8.5 - M_2)^2 + a_6(M_w - M_2) + a_7(M_w - M_2)^2 + [a_2 + a_3(M_w - M_1)]\ln R + a_{17} R_{RUP}$ where a_1, a_2, a_3, a_4, a_6, a_7, a_8, a_9, a_{17}, M_1, M_2 are period-dependent regression coefficients, and $R{=}R = \sqrt{R_{RUP}^2 + 1}$.	$M_w \leq 4$
BSSA14	$F_E = e_0 U + e_1 SS + e_2 NS + e_3 RS + e_4(M_w - M_h) + e_5(M_w - M_h)^2$ where U, SS, NS and RS are dummy variables being 0 or 1 depending on fault type, e_0-e_5 and M_h are period dependent regression coefficients.	$M_w \leq M_h$ $M_h = 5.5–6.2$
Yun08	$c_1 + c_2 M_L + (c_3 + c_4) M_L \times (\ln(R + c_9 \exp(c_5))) + c_6(M_L - 6)^2$ where c_1, c_2, c_3, c_4, c_5, c_6, c_9 are regression coefficients, and $R = \sqrt{R_{epi} + 9.8^2}$.	–

to the regression coefficients representing the source-to-site distance scaling of the existing GMMs, whereas at the borehole stations the slopes were generally smaller than the regression coefficients of the existing GMMs. This finding is in contrast with the observation in Ahn et al. (2021), where the slopes of IMs vs. R_{hypo} for recorded data were overall greater than the regression coefficients of the existing GMMs. This suggests that the attenuation of the ground motions recorded on Jeju Island is faster than in the region studied by Ahn et al. (2021), which is located in the southwestern part of inland South Korea. We attribute this stronger attenuation of ground motions to the presence of Seogwipo and U Formations. Further studies are necessary to explore the influence of these formations on the attenuation of ground shaking through detailed site characterization and seismic wave propagation analyses.

The 2021 M_L4.9 Jeju earthquake was a remarkable event with a series of aftershocks that provided valuable data to elucidate how the ground motions are influenced by the volcanics overlying soft sediments. However, this preliminary study has still been limited by the small number of available data. This study only considered M_L up to 4.9 and analyzed limited amount of data for $M_L > 2$. Analyzed data were also from earthquakes with a limited range of source-to-site distance (R_{hypo} between 16 and 100 km). Therefore, one should be cautious about utilizing magnitude and distance scaling suggested in this study. Nonetheless, it is anticipated that the magnitude and distance scaling derived from this study will be useful for developing a GMM specific to Jeju Island in the future, preferably with collection of more data that can cover wider magnitude and distance ranges.

CRediT authorship contribution statement

Youngkyu Cho: Writing – review & editing, Writing – original draft, Investigation, Funding acquisition, Formal analysis. **Seongnoh Ahn:** Visualization, Investigation, Data curation. **Junyoung Lee:** Validation,

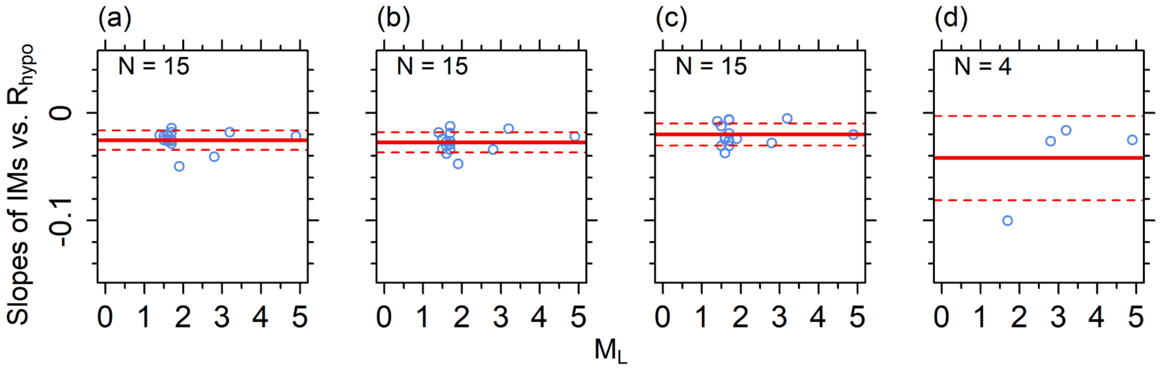

Fig. 12. The slope of hypocenter distance against various intensity measures for records of surface stations' seismograph: (a) PGA, (b) PGV, (c) $Sa^{0.2s}$, (d) Sa^{1s}.

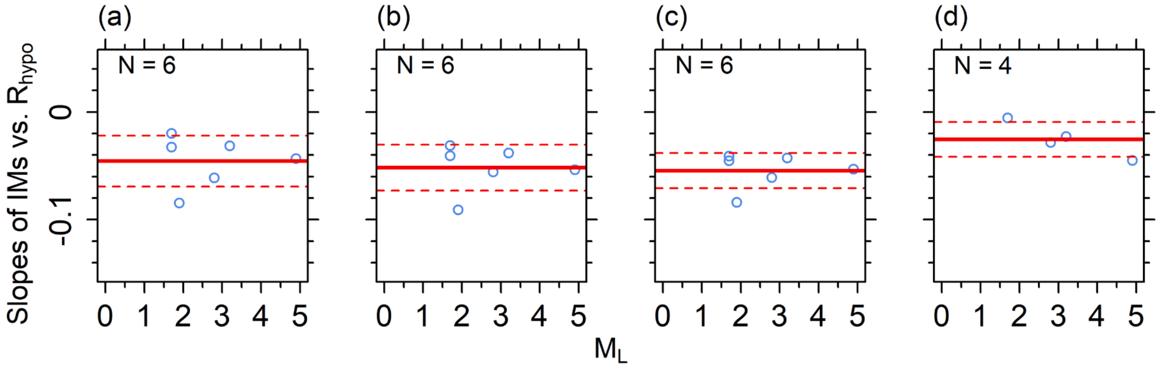

Fig. 13. The slope of hypocenter distance against various intensity measures for records of borehole stations' seismograph: (a) PGA, (b) PGV, (c) $Sa^{0.2s}$, (d) Sa^{1s}.

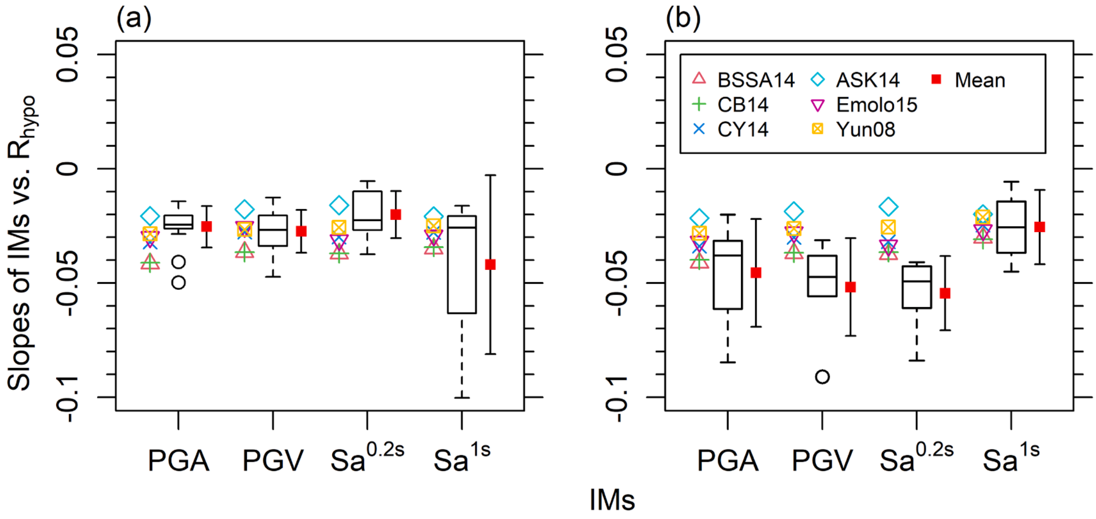

Fig. 14. The slope of R_{hypo} against the four intensity measures (i.e., PGA, PGV, $Sa^{0.2s}$, Sa^{1s}) for (a) surface and (b) borehole stations, respectively.

Data curation. **Jaehwi Kim:** Investigation, Data curation. **Byungmin Kim:** Writing – review & editing, Funding acquisition, Conceptualization. **Seokho Jeong:** Writing – review & editing, Supervision, Methodology, Funding acquisition, Formal analysis, Conceptualization.

Declaration of competing interest

The authors declare that they have no known competing financial interests or personal relationships that could have appeared to influence the work reported in this paper. Byungmin Kim is an Associate Editor of KSCE Journal of Civil Engineering.

Acknowledgments

This work was supported by the Korea Meteorological Administration (KMA) Research Development Program (grant number KMI2022-00610) and Basic Science Research Programs through the National Research Foundation of Korea (NRF), funded by the Ministry of Science and ICT (2020R1F1A1076539) and the Ministry of Education (2021R1I1A1A01049397). The authors thank the anonymous reviewers for their constructive comments and insightful suggestions, which have significantly improved the original draft of this article. We are also grateful to Junsu Oh and Jinhyeong Park, who participated in the field experiments on Jeju Island.

Supplementary materials

Supplementary material associated with this article can be found, in the online version, at doi:10.1016/j.kscej.2024.100148.

References

Abrahamson, N. A., Silva, W. J., & Kamai, R. (2014). Summary of the ASK14 ground motion relation for active crustal regions. *Earthquake Spectra, 30*, 1025–1055. https://doi.org/10.1193/070913EQS198M

Ahn, J.-K., Kim, B., & Kwak, D (2021). Source and path effects of the ground motions recorded during the 2020 Haenam earthquake swarm in South Korea. *Geosciences Journal, 25*, 83–92. https://doi.org/10.1007/s12303-020-0048-1

Boore, D. M., Stewart, J. P., Seyhan, E., & Atkinson, G. M. (2014). NGA-West2 equations for predicting PGA, PGV, and 5% damped PSA for shallow crustal earthquakes. *Earthquake Spectra, 30*, 1057–1085. https://doi.org/10.1193/070113EQS184M

Campbell, K. W., & Bozorgnia, Y. (2014). NGA-West2 ground motion model for the average horizontal components of PGA, PGV, and 5% damped linear acceleration response spectra. *Earthquake Spectra, 30*, 1087–1115. https://doi.org/10.1193/062913EQS175M

Chiou, B. S.-J., & Youngs, R. R. (2014). Update of the Chiou and Youngs NGA model for the average horizontal component of peak ground motion and response spectra. *Earthquake Spectra, 30*, 1117–1153. https://doi.org/10.1193/072813EQS219M

Emolo, A., Sharma, N., Festa, G., Zollo, A., Convertito, V., Park, J. H., Chi, H. C., & Lim, I. S. (2015). Ground-motion prediction equations for South Korea Peninsula. *Bulletin of the Seismological Society of America, 105*, 2625–2640. https://doi.org/10.1785/0120140296

Kalkan, E. (2016). An automatic P-phase arrival-time picker. *Bulletin of the Seismological Society of America, 106*, 971–986. https://doi.org/10.1785/0120150111

Kim, B., Hashash, Y. M. A., Rathje, E. M., Stewart, J. P., Ni, S., Somerville, P. G., … Campbell, K. W. (2016). Subsurface shear wave velocity characterization using P-wave seismograms in central and Eastern North America. *Earthquake Spectra, 32*(1), 143–169. https://doi.org/10.1193/123013EQS299M

Kim, J.-K., Wee, S.-H., Yoo, S.-H., & Kim, K.-H. (2021). Characteristics of the vertical and horizontal response spectra of earthquakes in the Jeju Island Region. *Applied Sciences, 11*, 10690. https://doi.org/10.3390/app112210690

Kim, J., Kim, B., & Cho, H. (2020). Shear Wave Velocity Estimation in Korea Using P-Wave Seismograms. *KSCE Journal of Civil Engineering, 24*, 3650–3658. https://doi.org/10.1007/s12205-020-0752-4

Kim, J., Heo, G., Kwak, D., & Jeong, S. J. G. (2023). The relationship between bedrock depth and site fundamental frequency in the nakdonggang delta region, South Korea. *Geotechnics, 3*(3), 550–560.

Kim, J. H., Hwang, J. H., Lim, C. W., Kim, C. O., & Jeon, G. H. (2006). Hydrogeologic characteristics of Groundwater in Jeju Island's Annexes. In *the 6th 'Groundwater Academic Seminar* (in Korean).

Koh, G. W., Park, J. B., Kang, B. R., Kim, G. P., & Moon, D. C. (2013). Volcanism in Jeju Island. *Journal of the Geological Society of Korea (in Korean), 49*, 209–230. https://doi.org/10.14770/jgsk.2013.49.2.209

Konno, K., & Ohmachi, T. (1998). Ground-motion characteristics estimated from spectral ratio between horizontal and vertical components of microtremor. *Bulletin of the Seismological Society of America, 88*, 228–241. https://doi.org/10.1785/BSSA0880010228

Korea Meteorological Administration (KMA). (2013). *National Earthquake Comprehensive Information System (NECIS)*. Retreived from http://necis.kma.go.kr/.

Kwak, D., Ahn, J.-K., Seo, H., Kang, S., & Kim, B. (2022). Single-path ground motion amplifications during the 2020 Haenam, South Korea, swarm. *Bulletin of Earthquake Engineering, 20*, 4937–4959. https://doi.org/10.1007/s10518-022-01386-z

Lee, J., Kim, K.-H., Kang, S. Y., Son, M., & Kim, B. (2022). Shear-wave velocity map for Pohang Basin, South Korea, based on the P-wave seismogram method. *Earthquake Spectra, 38*, 2162–2182. https://doi.org/10.1177/87552930221076532

Nakamura, Y. (1989). A method for dynamic characteristics estimation of subsurface using microtremor on the ground surface. Railway Technical Research Institute. *Quarterly Reports, 30*(1).

Nizamani, Z. A., & Park, D. (2021). Testing ground-motion prediction equations against moderate magnitude earthquake data recorded in Korea. *Bulletin of the Seismological Society of America, 111*, 321–338. https://doi.org/10.1785/0120200095

ParkSEIS. (2016). '**Park Seismic LLC.**', In. 2 Balsam Circle, Shelton, USA.

Rathje, E. M., Abrahamson, N. A., & Bray, J. D. (1998). Simplified frequency content estimates of earthquake ground motions. *Journal of Geotechnical and Geoenvironmental Engineering, 124*, 150–159. https://doi.org/10.1061/(ASCE)1090-0241(1998)124:2(150)

SESAME. (2004). *Guidelines for the implementation of the H/V spectral ratio technique on ambient vibrations: Measurements, processing and interpretation* (No. WP21-Deliverable D23.12), European Commission – Research General Directorate.

Sheen, D. H., Kang, T. S., & Rhie, J. (2018). A local magnitude scale for South Korea. *Bulletin of the Seismological Society of America, 108*, 2748–2755.

Vantassel, J., Cox, B., Wotherspoon, L., & Stolte, A. (2018). Mapping depth to bedrock, shear stiffness, and fundamental site period at CentrePort, Wellington, using surface-wave methods: Implications for local seismic site amplification. *Bulletin of the Seismological Society of America, 108*(3B), 1709–1721. https://doi.org/10.1785/0120170287. July 2018.

Woo, K. S., Sohn, Y. K., Yoon, S. H., San Ahn, U., & Spate, A. (2013). *Jeju island geopark-a volcanic wonder of Korea*. Springer Science & Business Media.

Xia, J., Miller, R. D., & Park, C. B. (1999). *Estimation of near-surface shear-wave velocity by inversion of Rayleigh waves, 64* pp. 691–700). https://doi.org/10.1190/1.1444578

Yun, K.-H., Park, D.-H., Chang, C.-J., & Sim, T.-M (2008). Estimation of aleatory uncertainty of the Ground-Motion attenuation relation based on the observed data. In *Proceedings of the Earthquake Engineering Society of Korea Conference* (pp. 116–123). Seoul.